DEGRADATION OF *HOMESTEAD HOLLOW* AT THE *INSIGHT* LANDING SITE BASED ON THE DISTRIBUTION AND PROPERTIES OF LOCAL DEPOSITS.

John A. Grant[1], Nicholas H. Warner[2], Catherine M. Weitz[3], Matthew P. Golombek[4], Sharon A. Wilson[1], Mariah Baker[1], Ernst Hauber[5], Veronique Ansan[6], Constantinos Charalambous[7], Nathan Williams[4], Fred Calef[4], W. Thomas Pike[7], Alyssa DeMott[2], Megan Kopp[2], Heather Lethcoe[4], and Maria E. Banks[8]

[1]Center for Earth and Planetary Studies, National Air and Space Museum, Smithsonian Institution, 6th at Independence SW, Washington, DC, 20560,
[2]SUNY Geneseo, Department of Geological Sciences, 1 College Circle, Geneseo, NY 14454,
[3]Planetary Science Institute, 1700 East Fort Lowell, Tucson, AZ, 85719,
[4]Jet Propulsion Laboratory, California Institute of Technology, Pasadena, CA,
[5]German Aerospace Center (DLR), Institute of Planetary Research,
[6]University of Nantes, Laboratory of Planetary and Geodynamics,
[7]Imperial College, London, Department of Electrical and Electronic Engineering,
[8]NASA Goddard Space Flight Center, Greenbelt, MD.

Key Points:

Homestead hollow is a degraded impact crater that was modified by mostly eolian and lesser impact and mass-wasting processes.

Rocks on the western side of the hollow are ejecta emplaced during the formation of a nearby crater relatively early in hollow history.

Most hollow degradation occurred during the first ~0.1 Ga after formation, followed by limited exterior stripping and interior infilling.

Abstract: The *InSight* mission landed its scientific payload in *Homestead hollow*, a quasi-circular depression interpreted to be a highly degraded impact crater that is 27 m in diameter. The original pristine crater formed in a pre-existing impact-generated regolith averaging ~3 m thick and the surrounding ejecta deposit, consisting of coarse and mostly fine fragments, was in disequilibrium with local geomorphic thresholds. As a result, early, relatively rapid degradation by mostly eolian, and lesser impact processes and mass-wasting, stripped the rim and mostly infilled the hollow where sediments were sequestered. Early, faster degradation during the first ~0.1 Ga was followed by much slower degradation over the bulk of the 0.4-0.7 Ga history of the crater. Pulses of much lesser degradation are attributed to impacts in and nearby the hollow, which emplaced some rocks as ejecta and provided small inventories of fine sediments for limited additional infilling. Even lesser sediments were derived from the very slow production of fines via weathering of resistant basaltic rocks. Nevertheless, indurated regolith caps the sediment fill within the hollow and creates a relatively stable present-day surface that further sequesters infilling sediments from remobilization. The degradation sequence at *Homestead hollow* is like that established at the *Spirit* rover landing site in Gusev crater and points to the importance of eolian, and lesser impact and mass-wasting processes, in degrading volcanic surfaces on Mars over the past ~1 Ga.

Plain Language Summary: The *InSight* mission landed in a highly degraded impact crater dubbed *Homestead hollow* in Elysium Planitia on Mars. The hollow interior is quite flat and smooth, and mostly infilled by fine-grained sediments. Rocks are 2-3 times more numerous on the western side dubbed *Rocky Field*. The hollow lacks a raised rim but is marked by an increase in larger rocks. The distribution of windblown and impact materials within, around, and local to the hollow indicate degradation was mostly by wind stripping of fines from the rim and depositing them inside the hollow, with lesser contributions from impact and mass wasting processes. *Rocky Field* was likely formed by emplacement of ejecta during a nearby impact event occurring relatively soon after *Homestead hollow* formed. Most degradation occurred during the first ~0.1 Ga after hollow formation. Limited modification over most of hollow history was associated with small pulses of infilling and rock emplacement during/following nearby impact events and very slow weathering of basaltic rocks. Degradation at *Homestead hollow* is similar to the modification of small craters at the *Spirit* landing site in Gusev crater, which shows common geomorphic processes occurred on comparable surfaces in different places on Mars during the last ~1 Ga.

1. Introduction

The Interior Exploration using Seismic Investigations, Geodesy, and Heat Transport (*InSight*) mission (Banerdt and Russell, 2017; Banerdt et al., 2019; 2020) landed a scientific payload in western Elysium Planitia on the broad, volcanic or sedimentary, Hesperian transition unit between the highlands and lowlands. The region is bounded by Noachian highlands to the south and west and the Medusae Fossae Formation and younger Athabasca Valles lavas to the southeast and east (Tanaka et al., 2014). The landing site is located at 4.50° N, 135.62° E (Banerdt et al., 2019; 2020; Golombek et al., 2019a; Parker et al., 2019) in the northwest corner of a highly degraded 27 m-diameter impact crater informally named "*Homestead hollow*" (Golombek et al., 2019a; 2019b; 2020; Warner et al., 2019a; 2019b) (Fig. 1). Orbital, stereo High-Resolution Imaging Science Experiment (HiRISE) (McEwen et al., 2007) images (0.25 m-pixel), were used to create a Digital Elevation Model (DEM) with a horizontal and vertical precision of 1 m and ~0.1-0.2 m, respectively (Fergason et al., 2017), and confirms the interior of *Homestead hollow* is ~0.3 m below the surrounding exterior surface (Golombek et al., 2019a; 2019b; Warner et al., 2019a; 2019b). Although the hollow lacks an appreciable elevated rim relative to the surrounding surface, the margin shows a significant increase in roughness due to variable exposure of abundant, float or loose, cobble-to-boulder sized rocks (no bedrock outcrops are present) as compared to the relatively smooth interior (Grant et al., 2019a; 2019b) (Figs. 1 and 2). The hollow originally formed in a ~3 m deep impact-generated regolith (Golombek et al., 2017; 2018; Warner et al., 2017) likely capped by the distal ejecta of an older, very degraded ~100 m-diameter crater whose rim is located approximately 50 m (or one radius (R) of the larger crater) to the northeast of *Homestead hollow* (Fig. 1). There are also at least eight younger craters <10 m-diameter that are superposed on or near the hollow with others nearby (Figs. 1 and 2). This study analyzes the properties and distribution of local deposits as viewed by the lander and from orbit to constrain the modification history of *Homestead hollow*.

2. Background and Geologic Setting

Although *Homestead hollow* formed into basaltic-composition plains (Pan et al., 2020) that could be sedimentary or volcanic (Tanaka et al., 2014), as summarized by Golombek et al. (2017; 2018), Warner et al. (2017), and Pan et al., (2020), we favor a volcanic lava origin based on: 1) relative proximity to north-south trending wrinkle ridges; 2) the presence of degraded lobate flow margins in the region (Golombek et al., 2018); 3) a number of 10 to 100-m-scale rocky ejecta craters near the landing site showing ejected rocks with a low albedo which is consistent with a strong competent layer ~20-200 m deep (Warner et al., 2017), 4) occurrence of platy and ridged surface textures and possible lava inflation plateaus and volcanic vents (Pan et al., 2020); 5) rocks with a fairly uniformly fine-grained aphanitic texture (Golombek et al., 2019a; 2020); 6) an absence of any observable sedimentary structures in rocks at the landing site; and 7) evidence that the broader Hesperian transition unit (Tanaka et al., 2014) experienced an Early Amazonian-aged resurfacing event in the vicinity of the landing site that was probably linked to regionally occurring Amazonian volcanism (Warner et al., 2017).

Homestead hollow is one of many small craterforms in the vicinity of the lander that is visible from both the lander and in orbital data (Figs. 1 and 2). These craters are in varying stages of degradation (Golombek et al., 2019a; 2019b; Grant et al., 2019a; 2019b; Warner et al. 2019a; 2019b), ranging from nearly pristine to those like *Homestead hollow*, which are so degraded that they are almost unrecognizable (Sweeney et al., 2018; Warner et al., 2020a; 2020b). The degraded form of *Homestead hollow* records the processes responsible for its modification over time and validate interpretations of similar impact structures made using orbital data. Because the hollow occurs on a likely volcanic surface that appears generally similar to other widespread surfaces on Mars (Tanaka et al., 2014), information about the number and timing of active degradation processes can be relevant to understanding degradation occurring over other surfaces during relatively recent Martian history.

Homestead hollow is interpreted to be a simple crater, whose pristine form can be deduced by comparison with the expected morphometry of other simple craters. Unmodified simple craters are characterized by a bowl-shaped interior surrounded by a raised rim and an outward-thinning ejecta deposit that extends about a diameter (D) from the rim (Melosh, 1989). In addition, the ejecta around simple craters consists of mixed fragments whose size distribution show an exponential increase in number with decreasing size, consistent with a distribution associated with multiple impact fragmentation processes (Melosh, 1989) and is observed elsewhere on Mars (Golombek and Rapp, 1997; Grant et al., 2006b). As summarized from Sweeney et al. (2018) and Warner et al. (2020a; 2020b), morphologic classification of more than 2,000 craters up to ~5 km from the landing site reveals a predictable continuum from a pristine form to increasingly degraded, rocky ejecta (ejecta rocks visible in HiRISE images with a 0.25 m pixel-scale) craters to even more degraded, non-rocky ejecta craters (Classes 1 to 8). Class 1 craters represent the pristine, ideal case of an unmodified bowl-shaped simple crater and are extremely rare in the landing site. From Class 2 to Class 5, rocks become less continuously distributed in the ejecta, the crater rim lowers, and eolian bedforms organize against the crater rim and in the interior. By Class 4 and 5, the bedforms plane off to form a smooth interior unit, but remain trapped against an elevated rim. From Class 6 to Class 8, all craters lack rocks in their ejecta, segments of the rim become completely degraded, and bedforms are no longer trapped against the crater rims or within the interiors. Class 8 craters are quasi-circular hollows that show a near zero rim height. Specific morphometric parameters such as crater depth, rim height, slope, and curvature, measured from a 1 m HiRISE DEM, confirm the observational classification scheme and indicate progressive modification from Class 1 to Class 8 (Warner et al 2020a; 2020b). The data indicate slope decline of the rim and infilling from fresher classes to the most degraded Class 8. Rim curvature values range from convex-up slopes for fresher craters to near zero for Class 7 and Class 8 craters, consistent with increased rim lowering over time. Crater floor curvature values are strongly concave-up for the freshest craters and approach zero for Class 7 and 8 craters as a result of infilling over time. *Homestead hollow* is an example of the most degraded, Class 8 craterform (Warner et al., 2020a; 2020b).

The hollow likely formed ~0.4-0.7 Ga (Sweeney et al., 2018; Golombek et al., 2019a; Warner et al., 2020a; 2020b; Wilson et al., 2019) into an average ~3 m thick impact-derived regolith capping the underlying basaltic plain (Golombek et al., 2017; 2018; Warner et al., 2017). The present degraded expression of the hollow contrasts with an expected pristine impact morphology characterized by an initial depth of ~3-4 m, and rim height of ~1 m (Sweeney et al., 2018; Warner et al., 2020a; 2020b). Despite the degraded appearance of the hollow, however, the preserved morphology and distribution of rocks in and around the structure provides clues regarding the types and timing of processes responsible for its present expression.

3. Methods

The morphology and surface properties of *Homestead hollow* and its surroundings were assessed using orbital HiRISE data (0.25 m pixel-scale) and data from the Instrument Deployment Camera (IDC, angular resolution of 0.82 mrad/pixel at the center of the image) (Maki et al., 2018) and the Instrument Context Camera (ICC, angular resolution of 2.1 mrad/pixel at the center of the image) (Maki et al., 2018) onboard the *InSight* lander. In some cases, we also compared some of the expected morphometric characteristics of pristine simple impact craters, such as the extent of ejecta (Melosh, 1989), extent of ejecta rays (Baldwin, 1963), ejecta thickness relative to D (McGetchin et al., 1973), and largest expected rock size (Moore, 1971), versus what is observed in and nearby *Homestead hollow*.

From HiRISE, IDC, and ICC images, we examined the surrounding landscape to evaluate landforms diagnostic of various geomorphic processes. For example, identification of free-standing bedforms (e.g., *The Wave*, Fig. 2, Golombek et al., 2019a), or other smooth, bright deposits (typically within local lows) are interpreted to be dust covered eolian deposits (Figs. 1 and 2). Any rocky deposits bounding locally steeper slopes at the base of crater walls would be indicative of mass-wasting materials. Circular forms, especially those whose rims appear to show relief relative to the surrounding plains, are likely impact craters. We also classified loose or float rocks in the hollow and its surroundings as mostly exposed, partially exposed/embedded, or mostly buried, in an attempt to constrain where net stripping versus deposition occurred (the lander descent engines caused only microns of stripping beyond the immediate lander that extended to ~15-20 m (Williams et al., 2019)).

In general, there are more large rocks visible around and beyond the margin of the hollow in the degraded remains of the ejecta, and there is an easily defined and often abrupt (on the eastern side of the hollow) transition at the rim to relatively smaller/less exposed rocks within the interior (Fig. 2). Based on analogy with the ~1.9 km-diameter Lonar crater on Earth, impacts into basalt on Mars should produce ejecta where cobble-sized and larger rock fragments (>6.4 cm in diameter) are mostly equant to somewhat more disc, bladed, and rod-shaped (Kumar et al., 2014). We assume this is likely a reflection of the fine-grained, often broadly uniform nature of basalt and that additional impacts, as have occurred into the regolith at *Homestead hollow*, will further fragment the rocks without significantly changing the overall shape distribution. This statement is generally supported by median grain circularity ($4\pi\text{Area}/\text{Perimeter}^2$) and aspect ratio (ratio of short axis to long axis) of 0.9 and 0.71, respectively, for cm-scale rocks close inside *Homestead hollow* and

within ~1-2 m of lander (Weitz et al., 2019a). Unfortunately, the lack of stereo imagery for surfaces more than a few meters in front of the lander precludes measurement of most rock axes. Nevertheless, a sense of where exhumation or burial has occurred at *Homestead hollow* can be gained by characterizing the exposed cross-section of rocks as a proxy for visually determining whether they are mostly exposed, partially exposed, or mostly buried . Because these rocks are too large to be transported by the wind, they accumulate in situ as surrounding fines are deflated.

With these points in mind, mostly exposed rocks are defined as broad to somewhat symmetrical in cross-section and/or the lower edge of the rock was visible. Partially exposed or embedded rocks are embayed by fines, present a smaller or less symmetrical cross-section, and their lower edge is not visible. By contrast, mostly buried rocks are significantly embayed to the point where only the top, and/or very limited exposed cross-section, is observed.

4. Homestead Hollow and Local Environs

The view of *Homestead hollow's* surface and its surroundings, as seen in images from HiRISE and the IDC and ICC, highlight examples of recent and ongoing eolian and impact activity. For example, numerous relatively smooth and bright circular areas mark nearby hollows of a similar impact origin and often advanced degradation state (Grant et al., 2019b; Warner et al., 2020a; 2020b, Fig. 2). ICC images of the area to the southeast of the lander (Fig. 3) reveal *Homestead hollow* is filled with abundant fine-grained sediments (Golombek et al., 2020) and there are rare examples of possible ventifacts (e.g., the rocks dubbed "*Ace of Spades*" and "*Turtle rock,*" see Golombek et al., 2019a), both of which are consistent with past and ongoing eolian activity (Fig. 3). In addition, small impact craters in and on the margin of the hollow (e.g., *Corintito,* Fig. 2) have further excavated the uppermost surface and redistributed local materials. This includes impact gardening of the uppermost ~1 m to create local inventories of fines and eject rocks into, and around, the hollow.

More detailed measurements from the HiRISE DEM and stereo lander images from the IDC (up to 1 mm pixel-scale) show the hollow interior surface is quite flat down to the cm-scale (Figs. 2 and 3), and slopes <3° to the southeast (Golombek et al., 2019a; 2020). These conditions limit active mass-wasting with the possible exception of some very small areas along the walls of some of the small craters superposing the hollow. Neither the HiRISE images, the HiRISE DEM, ICC, or IDC images show any morphologic evidence of past water-driven transport or degradation (e.g., incised valleys, gullies, or alluvial fans).

Initial mapping using lander ICC and IDC images (Figs. 2 and 3) shows the surface of the hollow interior is dominated by mostly sand to pebble-sized fines (Golombek et al., 2019a; 2020; Weitz et al., 2019b) that is variably punctuated by mostly isolated gravel/pebbles and cobbles (Grant et al., 2019a; 2019b). There are more pebbles and cobbles (>2 cm) on the west part of the hollow dubbed "*Rocky Field*" (Golombek et al., 2019a) where there are ~2X-3X more cm-scale and larger fragments per m^2 than in front of the lander (Fig. 2). The lander rocket motors excavated ~10-20 cm deep, steep-walled (greater than repose angle, see Golombek et al., (2019a; 2020)), pits beneath the lander that are surrounded by relatively reddish, nearly equant debris clods (Ansan et al., 2019; Grant et al., 2019b; Hauber et al., 2019). In addition, the hole created by penetration of

Heat Flow and Physical Properties Package (HP^3, see Spohn et al., 2018), is bounded by walls that are locally vertical to overhanging (Golombek et al., 2019a; 2020). The walls of the lander rocket pits and HP^3 hole show wavy to relatively horizontal, resistant layers that sometimes include pebbles likely cemented in a finer-grained matrix. These resistant layers are indurated regolith, hereafter referred to as "duricrust". Similar cemented horizons are observed in HiRISE images of some nearby craters (Sweeney et al., 2018), as well as at other Martian landing sites (e.g., Arvidson et al., 2010). The immediate exterior margin of the hollow appears devoid of widespread fines and the hollow interior lacks traditional eolian bedforms (e.g., ripples, dunes). Dust removed from much of the interior hollow surface by engine blast during landing resulted in significant darkening of the surface (Williams et al., 2019), but there are bright bedforms on the horizon (e.g., *The Wave*, Fig. 2) and relatively brighter areas nearby associated with other impact craters (mostly ~10 m-diameter and smaller, Fig. 1). By analogy with the pre-landing, dusty, bright appearance of Homestead hollow (Williams et al., 2019) and the dust-covered and generally fine-grained deposits filling similar-sized, generally similar appearing craters in Gusev crater (Arvidson et al., 2004), these features (Fig. 2) likely relate to dust-covered deposits of mostly sand (Golombek et al., 2020).

Out of 1,180 rocks classified in and around the hollow (333 on rim, 847 in the interior), mostly exposed rocks represent ~70% of those seen on and beyond the rim relative to a total of 30% of mostly buried (1%) and partially exposed/embedded (29%) rocks combined (Fig. 4). By contrast, there is a greater combined percentage (58%) of mostly buried (9%) and partially exposed/embedded (49%) rocks inside the hollow relative to the percentage of mostly exposed rocks (42%) (Fig. 4).

It is difficult to detect, and therefore classify, some small rocks at greater distances, because rocks in the foreground block the assessment of rocks behind them (often obscuring the rock base), and the fixed view from the lander favors detection of small rocks that are nearby in the hollow. Moreover, the viewing angle may preclude detection of buried rocks beyond the edge of the hollow and probably contributes to the apparent paucity of buried rocks along and beyond the rim. Nevertheless, the substantially larger number of exposed rocks relative to embedded and buried rocks along and beyond the hollow rim, and the comparable dominance of mostly buried and embedded rocks relative to exposed rocks inside the hollow, indicates their relative abundances are probably real.

5. Degradation Processes

The morphologic features of *Homestead hollow* and nearby environs, coupled with the evidence of ongoing geomorphic processes, enable the degradation history to be established. For example, the preponderance of eolian and impact features in and around *Homestead hollow* confirms the importance of these processes in shaping the present landscape. Moreover, possible contributions to degradation by other processes can be established from clues gleaned from other nearby craters as viewed from orbit and from the lander. The detailed nature of degradation features in and nearby the hollow also allows establishment of the relative importance of each process over time.

Impact formation of the hollow at ~0.4-0.7 Ga (Sweeney et al., 2018; Golombek et al., 2019a; Warner et al., 2020a; 2020b; Wilson et al., 2019) further fragmented an existing regolith averaging

a few meters thick (Golombek et al., 2017; 2018; Warner et al., 2017) that was likely capped by the eroded remnants of the ~20 cm thick or less ejecta associated with the larger, older ~100 m-diameter crater that extended into the area (based on expected relationships between decreasing ejecta thickness with increasing distance beyond the rim, see Melosh, (1989) and McGetchin et al., (1973)). Expectations from ejecta at Meteor Crater on Earth (Grant and Schultz, 1993) and examples from Gusev crater (Grant et al., 2006b) indicate debris excavated during hollow formation created an ejecta deposit of mixed fragments of varying size distribution, but with many more small fragments relative to large fragments. The size distribution of rocks that can be measured near the lander (Charalambous et al., 2019) is consistent with expectations from multiple impact fragmentation (e.g., Grant et al., 2006b) and observations that the surface is characterized by relatively fewer large rocks compared with much more abundant finer fragments (Charalambous et al., 2019; Golombek et al., 2019a; 2019b; 2020; Weitz et al., 2019b). In general, comparison with nearby, relatively pristine craters of similar size to *Homestead hollow* (Fig. 5) shows that the initial form resembled relatively pristine craters at some other Mars landing sites (e.g., in Gusev crater, see Grant et al., 2004; Golombek et al., 2020) and resulted in an initial landform whose surface relief and grain properties were out of equilibrium with local eolian and mass-wasting geomorphic thresholds (Grant et al., 2004).

Given the mixed rock sizes characterizing the initial ejecta surface surrounding the hollow, the relative abundance of mostly exposed versus partially exposed/embedded versus mostly buried rocks can be used as an indicator of where finer material has been eroded or deposited (Figs. 2 and 4). Generally, there are more rocks exposing larger cross-sections outside the hollow relative to within the hollow. More specifically, the large number of exposed rocks around the exterior of the hollow reflects removal of intervening fines, whereas the abundance of embedded and mostly buried rocks in the hollow is due to infilling via deposition of fines.

Given the presently low surface slopes and complete absence of water-related degradation features, it can be concluded that the removal of the bulk of the fine-grained sediments from the rim was the result of eolian stripping. The corresponding increase in embedded and buried rocks within the depression of the hollow reflects resultant downwind deposition of these fines stripped from the rim to where they were protected from further transport. Nevertheless, eolian stripping of the rim and surrounding ejecta surfaces resulted in incomplete infilling of the hollow interior (Golombek et al., 2020) because prevailing, reversing northwest-southeast winds (Spiga et al., 2018) transported some fines downrange and not back into the hollow.

The eolian stripping of the rim at *Homestead hollow* and associated infilling of the crater are broadly comparable to those observed around small impact features formed into basaltic rubble around the *Spirit* landing site in Gusev crater (Golombek et al., 2006; Grant et al., 2004; 2006a; 2006b). Like at *Homestead hollow*, local ejecta surfaces around comparably sized craters in Gusev are deflated creating a 2X-10X concentration of exposed rocks along crater rims (Grant et al., 2004). Deposition of fines within the craters at Gusev is dominated by grain sizes similar to those in *Homestead hollow* (Weitz et al., 2019a) and results in fewer exposed/more buried rocks inside the craters (Grant et al., 2004; 2006a; 2006b).

Eolian degradation of the hollow rim slowed as the inventory of available fines decreased, surface lags were created, and the increased relief of remaining larger fragments created a boundary layer sufficient to slow near-surface winds and preclude further erosion of fines. As the inventory of fines around *Homestead hollow* was depleted, subsequent eolian degradation continued at a greatly diminished average rate, limited by the introduction of any additional fines following nearby impacts and the very slow weathering and breakdown of resistant basaltic rim rocks to create additional fines for transport. Eventually, this very slow degradation led to limited additional infilling and loss of the topographic rim around the hollow whose relict expression became characterized by abundant exposed rocks.

It is likely that early degradation along the initially relatively steep wall of the newly formed hollow enabled some gravity-driven slope processes, probably manifested as rocks shed from the rim and upper wall to form talus along the margin of the crater floor. However, HiRISE images of nearby and relatively pristine craters of similar size do not reveal obvious wall-bounding talus, thereby suggesting that early mass wasting was limited and subordinate to eolian modification. Any gravity-driven processes would have quickly waned as back-wasting of the crater wall and accumulation of any talus decreased wall slopes, that were further stabilized by increasing eolian infilling along and up the crater wall. This scenario is consistent with prior conclusions that crater infilling rates exceed wall back-wasting by an order of magnitude (Sweeney et al., 2018; Warner et al., 2020a; 2020b).

There is no systematic decrease in rock exposure inward of the hollow edge. Instead, the transition between the more exposed and often larger rocks on the rim to the relatively smaller rocks in the interior is typically easily defined and even abrupt around much of the east side of the hollow (Fig. 2). Collectively, these observations suggest that there was minimal talus from gravity-driven transport of large rocks beyond the immediate base of the crater wall during infilling. Moreover, the initial ~3-4 m depth of the depression relative to its present depth indicates that infilling exceeds the maximum expected fragment size of 0.9-2.8 m produced during crater formation (based on the relation between crater size and largest associated rock described in Moore (1971) and confirmed by the maximum meter-scale of rocks size observed around the hollow). Hence, rocks lining the original floor of the hollow are buried beneath the fill.

Ongoing impacts continue to play multiple roles in hollow degradation. Some impacts within or on the rim of the hollow result in direct modification during crater formation (e.g., *Corintito*, see Fig. 2). The general paucity and small size of the largest fragments around these craters supports the conclusion that these small craters are not accessing and ejecting new rocks from depth (Fig. 2), either via fragmenting/excavating rocks from bedrock or accessing coarse fragments within the deeper regolith. However, these small impacts do eject some pre-existing fragments during their formation and further garden the near-surface to depths of a meter or so. Nearby impacts can also enable short pulses of sediment transport and limited infilling when their formation exposes additional fines for transport. In some cases, nearby impacts can also result in direct emplacement of ejecta within the hollow (Fig. 2). Collectively, these ongoing effects of impact degradation result in random, small pulses of sediment influx that can also contribute to infilling.

While the average expected thickness of the regolith forming the near surface in the region around *Homestead hollow* is ~3 m (Golombek et al., 2017; 2018; Warner et al., 2017), some locales will be characterized by thinner or thicker deposits. In the vicinity of *Homestead hollow*, impacts of varying size occur randomly (as is typical on the surface of planets (Melosh, 1989). In the vicinity of the *InSight* lander, these randomly occurring impacts would disrupt the surface to varying depth from location to location, thereby resulting in differing thicknesses of regolith. For example, larger and/or multiple impacts in some locations will garden to greater depth than in locations where smaller/fewer impacts have occurred. Such expected variability in regolith thickness is accentuated where local occurrences of finer sequences are associated with infilling of any pre-existing craters. These factors create local substrates whose differing properties influence the susceptibility of small later forming impact craters (i.e., *Homestead hollow*-sized) to eolian degradation over time (Fig. 5).

Formation of some *Homestead hollow*-sized craters in thinner regolith that is less gardened by impacts may enable access to relatively more and larger rocks that are nearer the surface, whereas other craters forming within the generally more uniform, finer sediments infilling pre-existing craters will have access to fewer rocks (Fig. 5). This variability in target properties influences the resultant morphology and degradation of these small, strength-controlled craters (Melosh, 1989): those accessing bedrock or forming in rockier material may be less circular (on average) than those forming entirely within finer, pre-existing crater fill (Fig. 5). Eolian degradation will likely proceed more rapidly and completely in and around craters formed in mostly fines because fewer large rocks are present to form inhibiting lags and/or create sufficiently thick boundary layers to impede erosion.

6. Origin of *Rocky Field*

Based on the occurrence of the increased rock density covering the western portion of the hollow interior that forms *Rocky Field* (Figs. 1 and 2), several possible origins can be considered. The approximately circular morphology of the hollow coupled with the cross-hollow extent of *Rocky Field* suggests that it is probably not an offset portion of an irregular hollow rim or interior terrace created by impact into variable regolith materials (Warner et al. 2019a; 2019b) (Fig. 1) as is observed in some similar-sized craters in the vicinity (Fig. 5a and 5b). The cm-to-dm-scale size of the fragments comprising *Rocky Field* also rules out transport by eolian processes. The shallow depth, absence of slopes more than a few degrees, and lack of a systematic increase in rock burial away from the rim and the size of the fragments argues against a distribution related to mass wasting.

Rocky Field could be the ejecta (as part of a continuous, discontinuous, or ray deposit) related to a nearby impact event that post-dates the formation of the hollow. The presence of less degraded craters near *Homestead hollow* confirms such impacts have occurred. Impacts forming craters smaller than 10 m are likely too small to garden the regolith to sufficient depth or excavate/eject abundant rocks (e.g., consistent with the relative paucity of rocks around *Corintito*, *The Puddle*, and other m-scale craters superposing the hollow, see Fig. 2) and would need to have formed very

close to the hollow to directly emplace ejecta and form *Rocky Field*. Larger craters, however, could access and eject larger rocks and could also be located be farther away from the hollow.

If the rocks forming *Rocky Field* are part of a continuous or discontinuous ejecta deposit, their occurrence on only the western part of the hollow (Figs. 1 and 2) suggests any possible source crater would lie to the west and *Homestead hollow* would be close to 1D or less or slightly more than 1D of the parent crater, respectively (Melosh, 1989) (Fig. 6). By contrast, if *Rocky Field* is part of an ejecta ray, the source crater would be expected to be to the north or south of *Homestead hollow* and could be located farther away, given that rays can reach on order ~3D or $10.5R^{1.25}$ from the parent crater (Baldwin, 1963; Melosh, 1989). Using these criteria as a guide, a search was made around the hollow for younger craters located at the right distance and azimuth to account for the orientation of the *Rocky Field* boundary (Table 1, Fig. 6). Younger craters were defined as those having experienced lesser measurable amounts of modification than *Homestead hollow*, recognizing that some larger but somewhat more pristine craters have larger scale morphometric attributes that will survive an amount of degradation that would result in more complete destruction of the same features associated with smaller craters.

Several nearby craters were evaluated and ruled out as sources for *Rocky Field* (Table 1, Fig. 6). A younger Class 3, 100 m-diameter crater, located ~400 m east-southeast of *Homestead hollow* (Fig. 6) was ruled out because: 1) *Rocky Field* is on the west side of *Homestead hollow* and there is a paucity of rocks on the east side and closer to the Class 3 crater; 2) the Class 3 crater is too far away to have sourced *Rocky Field* as either continuous or discontinuous ejecta (Melosh, 1989); and 3) any rays associated with the crater would not have reached *Homestead hollow*, and even if they had they would have been oriented approximately orthogonal to boundary of *Rocky Field*. A younger 130 m-diameter Class 5 crater ~700 m to the east-northeast of *Homestead hollow* is also too far away to have emplaced ejecta or rays, and any rays would that would have reached *Homestead hollow* would be orthogonal to the *Rocky Field* boundary. Younger Class 6 craters (125 m-diameter and 440 m to the north, 80 m-diameter and 250 m to the south) are at favorable azimuths relative to *Homestead hollow* to form rays with orientations consistent with *Rocky Field*, but are too far away to have contributed continuous or discontinuous ejecta, or rays (Table 1). Two Class 7 craters, one located 250 m south-southwest of *Homestead* (80 m-diameter) and one located 510 m to the north (125 m-diameter), both predate the hollow and were also ruled out as possible sources.

Several other craters are possible sources of the rocks in *Rocky Field* (Table 1). The first is a ~15 m-diameter Class 8 hollow/craterform ~15 m west of *Homestead hollow* (Figs. 1 and 5). Although approximately as degraded as Homestead, this smaller hollow/crater required lesser degradation to achieve Class 8 status and is likely slightly younger than Homestead. The crater may have excavated to sufficient depth to eject rocks, but the far edge of *Rocky Field* in the hollow is located up to ~1.5-2.0D beyond its rim, likely beyond the expected extent of the continuous ejecta deposit associated with the crater (Melosh, 1989) and it is unclear whether discontinuous ejecta would be expected to extend to such a range. Any rays associated with the crater could extend

~50-60 m beyond the rim (Baldwin, 1963) and reach *Homestead hollow*, but the north-south orientation of the *Rocky Field* boundary is orthogonal to the expected ray orientation and therefore the crater is an unlikely source of *Rocky Field*.

A 110 m-diameter Class 5 crater ~280 m northwest of *Homestead hollow* is slightly younger than the hollow and likely formed ~400 Myr ago (Sweeney et al., 2018; Warner et al., 2020a; 2020b). Although the crater is too far away to have emplaced rocks associated with its continuous or discontinuous ejecta deposit, it is possible that a ray from the crater could have reached the hollow. It is unclear, however, whether the likely northwest-southeast orientation of any possible ray deposit would match the more north-south boundary of *Rocky Field*.

Finally, a degraded (Class 6, see Fig. 6 and Warner et al., 2020a; 2020b) ~100 m-diameter impact structure approximately 100 m northwest of *Homestead hollow* is an example of a rocky ejecta crater that is surrounded by numerous m-scale rocks excavated from more competent material below the bulk of the regolith (Warner et al., 2017) and is likely younger than the hollow. The crater has a probable retention age of ~0.4-0.6 Ga (Warner et al., 2020a; 2020b) and, although it is relatively well-preserved compared to the hollow, comparable amounts of degradation at both could result in the more degraded appearance of the hollow. Hence, *Homestead hollow* could be on order of ~0.1 Ga older than the crater to the northwest (Warner et al., 2020a; 2020b).

Homestead hollow is located ~1.2D from the ~100 m-diameter crater to the northwest and is likely beyond the limit of the continuous ejecta blanket. However, discontinuous ejecta deposits can extend to greater range (Melosh, 1989) and could account for *Rocky Field*. Discontinuous ejecta around Meteor Crater in Arizona, also a simple crater, is observed at a comparable distance north-northwest of the crater (Grant and Schultz, 1993). Like *Rocky Field*, the Meteor Crater deposits are characterized by patchy to irregularly scattered concentrations of rocks (Grant and Schultz, 1993). Hence, the best overall candidate source crater for the origin of *Rocky Field* is the Class 6 crater 100 m to the northwest whose discontinuous ejecta may have reached into the hollow. Nevertheless, the small Class 8 crater immediately to the west, and the Class 5 crater 280 m to the northwest, cannot be definitively ruled out as sources for *Rocky Field* (Table 1).

7. Timing of Degradation

Multiple observations indicate that *Homestead hollow* and other similar-sized craters transition from a pristine impact crater to a significantly more degraded Class 5 crater at least three to six times faster than the transition from Class 5 to Class 8. Moreover, degradation occurring during the pristine to Class 5 transition is much more significant than the degradation that occurs during the transition from Class 5 to Class 8, but both intervals are dominated by eolian stripping of the crater exterior that removes much of the rim, lesser impact contributed sediments, and are accompanied by at least ~3 m of total infilling (Fig. 6).

First, assessment of craters within 5-6 km of *InSight* using HiRISE data (Fig. 5) confirms an absence of pristine morphologies in the size-range of *Homestead hollow*. By contrast, there are multiple examples of initially degraded craters that are similar in size to *Homestead hollow* that are characterized by at least some infilling often partially capped by small eolian ripples (e.g., Class 2 and 3, see Fig. 5). The inventory of initially modified craters is consistent with expectations

of ongoing crater formation (Warner et al., 2020a; 2020b), but confirms they must undergo early rapid degradation to account for the paucity of pristine forms (Fig. 7).

The probable origin and survival of *Rocky Field* as ejecta arriving from a nearby crater early in hollow history further requires significant preceding infilling to something close to what is currently observed. All three candidate crater sources for *Rocky Field* (Table 1) are degraded and nearly as old as *Homestead hollow*, thereby requiring emplacement of the fragments forming *Rocky Field* early in hollow history. And even if one of the other Class 6 craters considerably further to the north-northwest or to the south produced rays extending well beyond predictions (Table 1) and that reached the hollow to create *Rocky Field*, they are nearly as old as *Homestead* and also require early emplacement of the rocks. By contrast, the continued exposure of the rocks in *Rocky Field* points to minimal additional infilling and long-term stability of the hollow interior since they were emplaced.

Examination of IDC images does not reveal divots, rolling or bouncing tracks, or other evidence likely associated with ballistic emplacement of the fragments in *Rocky Field*, thereby requiring some post-arrival modification of the surface. Continued exposure of the constituent rocks, however, limits appreciable post-emplacement net infilling of the hollow from centimeters to perhaps a couple of decimeters. Moreover, the well-defined nature of *Rocky Field* coupled with its likely impact origin early in hollow history implies there was limited time for emplacement of additional ejecta horizons within the hollow fill prior to its formation (Fig. 7). Other small scattered fragments across the hollow interior and outside of *Rocky Field* are consistent with one or multiple later ejecta emplacement events, but none that were comparable in scale to the one forming *Rocky Field*. Finally, the presence of rare, possible ventifacts within the hollow (e.g., *Turtle rock* and *Ace of Spades* rock, Fig. 3) and occurrence of duricrust material in the uppermost fill (Golombek et al., 2019a; 2020) supports long-term stability of the present hollow surface and/or potential net bypassing of most sediment since it was established. Based on local crater retention studies (Sweeney et al., 2018; Warner et al., 2020a; 2020b), the transition from a pristine impact to more degraded Class 5 and most hollow infilling likely occurred within the first ~0.1 Ga of crater formation (Fig. 7, Warner et al., 2020a; 2020b) consistent with the contention that most hollow degradation occurred over a relatively short period following impact formation.

The hollow retention age of 0.4-0.7 Ga (Warner et al., 2019a; 2019b) indicates that the subsequent ~0.3-0.6 Ga hollow history saw only minor degradation that eventually accounted for the slow morphologic transition from a Class 5 to Class 8 crater. After early crater infilling (Fig. 5), degradation rates greatly slowed as the inventory of available fines for transport from the rim into the hollow became limited. Exterior surfaces were stabilized by development of coarse lags and/or when stripping left larger fragments standing in greater relief and created a sufficiently thick boundary layer to preclude motion of fines. Any additional late stage stripping of the rim was very limited and related to the extremely slow production of fines via weathering of resistant basaltic-composition rocks.

At late stages of degradation, small impacts into and around the hollow, and associated local impact gardening to a meter or so, exposed few rocks and created limited additional inventories of

fines for transport (Figs. 1, 2, and 6), but did not result in significant hollow infilling. Moreover, as nearly complete infilling reestablished a surface profile close to equilibrium with local winds, longer-term surface stability was enhanced. Development of cemented soils or duricrust hardened the surface, sequestered most of the sediment inventory within the hollow, and further limited ongoing modification or remobilization of infilling sediments during rare high wind events. Duricrust development in *Homestead hollow* may have been similar to postulated duricrust formation in Gusev crater where thin films of water associated with frost or snowpack development (perhaps during periods of high obliquity) played a key role (Arvidson et al., 2010). Nevertheless, the relatively high albedo of the interior of *Homestead* (mostly beyond the blast zone of the lander) and other nearby hollows as well as the bright appearance of *The Wave* bedforms suggests they are covered by dust and presently inactive (Sullivan et al., 2008; Golombek et al. 2010).

The partially exposed/embedded appearance of many fragments in the hollow indicates limited long-term infilling. And the stratigraphy exposed by rocket motors during landing includes what appear to be some hard fragments mixed with duricrust and duricrust clods (Golombek et al., 2019a). Nevertheless, the example of *Rocky Field* shows that these fragments are not rooted to the crater floor and arrived after infilling was largely complete (Fig. 7), thereby limiting total infilling over most of the hollow history to no more than a decimeter or two. The extremely slow rate of ongoing infilling of the remaining ~0.3 m deep depression associated with the hollow supports establishment of a profile nearly in equilibrium with local geomorphic processes.

Nearby craters that are similar in size to *Homestead hollow*, but formed in more rocky, thinner regolith, would also undergo fairly rapid early degradation, but occurrence of more abundant/larger rocks in the surrounding ejecta would result in faster development of lags armoring/protecting the surface after lesser stripping than at *Homestead hollow* and would mean there would be lesser early infilling and a quicker transition to slower, longer-term degradation than at *Homestead hollow*. By contrast, similar-sized craters formed in the pre-existing, finer-grained fill of older craters would be surrounded by ejecta with fewer rocks. As a result, the ejecta around these craters could experience greater stripping before any formation of an armoring/protecting surface. Hence, craters formed in finer substrates may undergo more sustained, faster stripping, complete infilling, and faster erasure.

Like at *Homestead hollow*, small craters on the floor of Gusev crater experienced early eolian and slope-driven degradation and then transitioned to much slower modification in a sequence roughly comparable to what is observed at *Homestead hollow* (Grant et al., 2004; 2006a; 2006b; Golombek et al., 2006). On the plains in Gusev, small craters of a range of sizes formed into a basaltic regolith setting broadly similar to the *InSight* landing site (e.g., Grant et al., 2004; Golombek et al., 2018; Weitz et al., 2019a). Crater rims in Gusev appear slightly better defined (topographically) in HiRISE views than in the vicinity of *InSight* and there appears to be more relatively darker sands on the Gusev plains (Weitz et al., 2019a). Nevertheless, the first order range in morphology of small craters is quite similar in both locations. The Gusev craters are also degraded by mostly eolian and lesser impact and mass-wasting that included eolian stripping of fine-grained sediments from around their rims and associated downwind deposition and infilling of

their interiors (Grant et al., 2004; Golombek et al., 2006). Moreover, the crater fill in the Gusev craters is capped by surface crusts (Arvidson et al., 2004) that resemble the duricrust in Homestead hollow and there is limited net erosion in the present environment (Grant et al., 2004), thereby indicating that Gusev hollow surfaces have been relatively stable for an extended period. Hence, most of the small crater degradation at Gusev likely took place relatively shortly after impact formation when sediments became available for transport and on a general timeline analogous to degradation at the *InSight* landing site. Given that volcanic surfaces are fairly widespread on Mars (Tanka et al., 2014), the mostly impact, eolian, and lesser mass wasting degradation and history defined at the *InSight* landing site may be representative of widely occurring degradation occurring on Mars over at least the past 1 Ga.

Acknowledgements

We thank the Jet Propulsion Lab, Lockheed Martin Space Systems, CNES, and other partner institutions that built and operate the *InSight* lander. A portion of the work was supported by the *InSight* Project at the Jet Propulsion Laboratory, California Institute of Technology, and under grants 80NSSC18K1625 to J. Grant (includes C. Weitz and S. Wilson) and 80NSSC18K1624 to N. Warner from the National Aeronautics and Space Administration. The data used are listed in the figures and (or) repository atSmithsonian.figshare.com doi:10.25573/data.11774598. This is *InSight* Contribution Number 146.

References:

Ansan, V., Hauber, E., Golombek, M. P., Warner, N. H., Grant, J. A., Maki, J., Deen, R., Calef, F., et al. (2019), *InSight* landing site: Subsurface stratigraphy and implications for formation processes, *9th Intl Mars Conf.*, 6050, LPI, Houston, TX.

Arvidson, R. E., Anderson, R. C., Bartlett, P., Bell, J. F., III, Blaney, D., Christensen, P. R., Chu, P., Crumpler, L., et al. (2004), Localization and physical properties experiments conducted by Spirit at Gusev Crater, *Science*, 305, 821-824. doi: 10.1126/science.1099922.

Arvidson, R. E., Bell, J. F., III, Bellutta, P., Cabrol, N. A., Catalano, J. G., Crumpler, L., Des Marais, D. J., Estlin, T., et al. (2010), Spirit Mars Rover Mission: Overview and Selected Results from the Northern Home Plate Winter Haven to the Side of Scamander Crater, *Journal of Geophysical Research*, 115, E00F03. https://doi.org:10.1029/2010JE003633.

Baldwin, R. B. (1963), *The Measure of the Moon*, University of Chicago Press, Chicago, IL.

Banerdt, W. B., Russell, C. T. (2017), Editorial on: Topical Collection on *InSight* Mission to Mars, *Space Science Reviews*, 211, 1–3. https://doi.org/10.1007/s11214-017-0414-0.

Banerdt, W. B., Smrekar, S., Antonangeli, D., Asmar, S., Banfield, D., Beghein, C., Bowles, N., Bozdag, E., et al. (2019), *InSight* – The first three months on Mars, *LPSC L*, 2132, LPI, Houston, TX.

Banerdt, W. B., Smrekar, S., Banfield, D., Giardini, D., Golombek, M., Johnson, C., Lognonne, P., Spiga, A., et al. (2020), Early results from the *InSight* mission: Mission overview and global seismic activity, *Nature Geosciences*. https://doi.org/10.1038/s41561-020-0544-y.

Calef, F. J., III, Soliman, T., Abarca, H. E., Deen, R., Ruoff, N., Williams, N., Berger, L., Lethcoe-Wilson, H., et al. (2019), Science operations with the *InSight* WebGIS, *LPSC L*, 1977, LPI, Houston, TX.

Charalambous, C., Golombek, M. P., Pike, T., Warner, N. H., Weitz, C. M., Ansan, V., Hauber, E., Grant, J. A., et al. (2019), Rock distribution at the *InSight* landing site and implications based on fragmentation theory, *LPSC L*, 2812, LPI, Houston, TX.

Fergason, R. L., Kirk, R. L., Cushing, G., Galuzska, D. M., Golombek, M. P., Hare, T. M., Howington-Kraus, E., Kipp, D. M., et al. (2017), Generation of digital elevation models and analysis of local slopes at the *InSight* landing site region, *Space Science Reviews*., 211, 109–133. https://doi.org:10.1007/s11214-016-0292-x.

Golombek, M., and Rapp, D. (1997), Size-frequency distributions of rocks on Mars and Earth analog sites: Implications for future landed missions, *Journal of Geophysical Research*,102, 4117–4129.

Golombek, M. P., Grant, J. A., Crumpler, L. S., Greeley, R., Arvidson, R. E., Bell, J. F., III, Weitz, C. M., Sullivan, R., et al. (2006), Erosion rates at the Mars Exploration Rover landing sites and long-term climate change on Mars, *Journal of Geophysical Research*, 111, E12S10. https://doi.org:10.1029/2006JE002754.

Golombek, M. P., Robinson, K., McEwen, A., Bridges, N., Ivanov, B., Tornabene, L., Sullivan R., (2010), Constraints on ripple migration at Meridiani Planum from Opportunity and HiRISE observations of fresh craters, *Journal of Geophysical Research*, 115, E00F08. https://doi.org:10.1029/2010JE003628.

Golombek, M. P., Kipp, D., Warner, N., Daubar, I. J., Fergason, R., Kirk, R., Beyer, R., Huertas, A., et al. (2017), Selection of the *InSight* landing site, *Space Science Reviews*, 211, 5–95. https://doi.org/10.1007/s11214-016-0321-9.

Golombek, M. P., Grott, M., Kargl, G., Andrade, J., Marshall, J., Warner, N., Teanby, N. A., Ansan, V., et al. (2018), Geology and physical properties investigations by the *InSight* lander, *Space Science Reviews*, 214, 84. https://doi.org/10.1007/s11214-018-0512-7.

Golombek, M. P., Warner, N. H., Grant, J. A., Hauber, E., Ansan, V., Weitz, C. M., Williams, N., Charalambous, C., et al. (2019a), Geology of the *InSight* landing site Mars: Initial observations, *LPSC L*, 1694, LPI, Houston, TX.

Golombek, M. P., Warner, N. H., Grant, J. A., Hauber, E., Ansan, V., Weitz, C. M., Williams, N., Charalambous, C., et al. (2019b), Geology of the *InSight* landing site Mars, *9th Intl Mars Conf.*, 6106, LPI, Houston, TX.

590 Golombek, M. P., Warner, N. H., Grant, J. A., Hauber, E., Ansan, V., Weitz, C. M., Williams, N.,
591 Charalambous, C., et al. (2020), Geology of the *InSight* landing site on Mars, *Nature Com-*
592 *munications*. https://doidoi.org: D10.1038/s41467-020-14679-1.

593 Grant, J. A., and Schultz, P. H., (1993), Erosion of Ejecta at Meteor Crater, Arizona, *Journal of*
594 *Geophysical Research*, 98, 15,033-15,047.

595 Grant, J. A., Arvidson, R. E., Bell, J. F., III, Cabrol, N. A., Carr, M. H., Christensen, P. R., Crum-
596 pler, L., Des Marais, D. J., et al. (2004), Surficial deposits at Gusev Crater along Spirit
597 rover traverses, *Science*, 305, 807-810. https://doi.org: 10.1126/science.1099849.

598 Grant, J. A., Arvidson, R. E., Crumpler, L. S., Golombek, M. P., Hahn, B., Haldemann, A. F. C.,
599 Li, R., Soderblom, L. A., Squyres, S. W., et al. (2006a), Crater gradation in Gusev crater
600 and Meridiani Planum, Mars, *Journal of Geophysical Research*, 111.
601 https://doi.org:10.1029/2005JE002465.

602 Grant, J. A., Wilson, S. A., Ruff, S. W., Golombek, M. P., and Koestler, D. L. (2006b), Distribution
603 of rocks on the Gusev Plains and on Husband Hill, Mars, *Geophysical Research Letters*,
604 33, L16202. https://doi.org:10.1029/2006GL026964.

605 Grant, J. A., Warner, N. H., Weitz, C. M., Golombek, M. P., Wilson, S. A., Hauber, E., Ansan, V.,
606 Charalambous, C., et al (2019a), Modification of *Homestead hollow* at the *InSight* landing
607 site based on the distribution and properties of local deposits, *LPSC L*, 1199, LPI, Houston,
608 TX.

609 Grant, J. A., Warner, N. H., Weitz, C. M., Golombek, M. P., Wilson, S. A., Hauber, E., Ansan, V.,
610 Charalambous, C., et al. (2019b), Modification of *Homestead hollow* at the *InSight* landing
611 site based on the distribution and properties of local deposits, *9th Intl Mars Conf.*, 6207,
612 LPI, Houston, TX.

613 Hauber, E., Ansan, V., Szczech, C., Adeli, S., Golombek, P., Warner, N., Charalambous, C., Grant,
614 J., et al (2019), Geology of the *InSight* landing site, Mars: Initial results, *EPSC-DPS Joint*
615 *Meeting 2019*, EPSC-DPS2019-1794, Berlin, DE.

616 Kumar, P. S., Prasanna Lakshmi, K. J., Krishna, N., Menon, R., Sruthi, U., Keerthi, V., Senthil
617 Kumar, A., Mysaiah, D., et al. (2014), Impact fragmentation of Lonar Crater, India: Impli-
618 cations for impact cratering processes in basalt, *Journal of Geophysical Research*, 119,
619 2029–2059. https://doi.org:10.1002/2013JE004543.

620 Lognonné, P., Banerdt, W. B., Giardini, D. Pike, W. T., Christensen, U., Laudet, P., de Raucourt,
621 S., Zweifel, P., et al. (2019), SEIS: *InSight*'s Seismic Experiment for Internal Structure of
622 Mars, *Space Science Reviews*, 215, 12. https://doi.org/10.1007/s11214-018-0574-6

623 Maki, J., Golombek, M. P., Deen, R., Abarca, H., Sorice, C., Goodsall, T., Lemmon, M., Trebi-
624 Ollennu, A., et al. (2018), The color cameras on the *InSight* lander, *Space Science Reviews*,
625 214, 105. https://doi.org:10.1007/s11214-018-0536-z.

McEwen, A. S., Eliason, E. M., Bergstrom, J. W., Bridges, N. T., Hansen, C. J., Delamere, W. A., Grant, J. A., Gulick, V. C., et al. (2007), Mars Reconnaissance Orbiter's High Resolution Imaging Science Experiment (HiRISE), *Journal of Geophysical Research*, 112, E05S02. https://doi.org:10.1029/2005JE002605.

McGetchin, T. R., Settle, M., and Head, J. W. (1973), Radial thickness variation in impact crater ejecta: Implications for lunar basin deposits, *Earth and Planetary Science Letters*, 20, 226–236. https://doi.org:10.1016/0012-821X(73)90162-3.

Melosh, H. J. (1989), *Impact cratering*, New York, Oxford University Press, 245 p.

Moore, H. J. (1971). Large blocks around lunar craters, in Analysis of Apollo 10 Photography and Visual Observations. *NASA Special Publication*, SP-232, 26–27.

Pan, L., Quantin-Nataf, Q., Tauzin, B., Michaut, C., Golombek, M. P., Lognonne, P., Grindrod, P., Langlais, B., et al. (2020), Crust stratigraphy and heterogeneities of the first kilometers at the dichotomy boundary in western Elysium Planitia and implications for *InSight* lander, *Icarus*, 338. https://doi.org/10.1016/j.icarus.2019.113511

Parker, T. J., Golombek, M. P., Calef, F. J., Williams, N. R., LeMaistre, S., Folkner, W., Daubar, I. J., Kipp, D., et al. (2019), Localization of the *InSight* lander, *LPSC L*, 1948, LPI, Houston, TX.

Spiga, A., Banfield, D., Teanby, N. A., Forget, F., Lucas, A., Kenda, B., Rodriguez-Manfredi, J. A., Widmer-Schnidrig, R., et al. (2018), Atmospheric science with *InSight*, *Space Science Reviews*, 214, 109. https://doi.org:10.1007/s11214-018-0543-0.

Spohn, T., Grott, M., Smrekar, S. E., Knollenberg, J., Hudson, T. L., Krause, C., Muller, N., et al. (2018), The heat flow and physical properties package (HP^3) for the *InSight* mission, *Space Science Reviews*, 214, 96. https://doi.org/10.1007/s11214-018-0531-4.

Sullivan, R., Arvidson, R., Bell, J. F., III, Gellert, R., Golombek, M. P., Greeley, R., Herkenhoff, K. E., Johnson, J., et al. (2008), Wind-driven particle mobility on Mars: *InSight* from Mars Exploration Rover observations at "El Dorado" and surroundings at Gusev crater, *Journal of Geophysical Research*, 113. E06S07. https://doi.org:10.1029/2008JE003101

Sweeney, J., Warner, N. H., Ganti, V., Golombek, M. P., Lamb, M. P., Fergason, R., and Kirk, R. (2018), Degradation of 100-m-scale rocky ejecta craters at the *InSight* landing site on Mars and implications for surface processes and erosion rates in the Hesperian and Amazonian, *Journal of Geophysical Research*, 123, 2732. https://doi.org/10.1029/2018JE005618.

Tanaka, K., Skinner, J. A., Jr., Dohm, J. M., Irwin, R. P., III, Kolb, E. J., Fortezzo, C. M., Platz, T., Michael, G. G., et al. (2014), Geologic map of Mars, *United States Geological Survey Science Investigations*, Map 3292.

Warner, N. H., Golombek, M. P., Sweeney, J., Fergason, R., Kirk, R., Schwartz, C. (2017), Near surface stratigraphy and regolith production in southwestern Elysium Planitia, Mars: Implications for Hesperian-Amazonian terrains and the *InSight* lander mission, *Space Science Reviews*, 211, 147-190. https://doi.org/10.1007/s11214-017-0352-x.

Warner, N. H., Golombek, M. P., Grant, J. A., Wilson, S. A., Hauber, E., Ansan, V., Weitz, C., Charalambous, C., et al. (2019a), Geomorphology and origin of *Homestead hollow*, the landing location of the *InSight* lander on Mars, *LPSC L*, 1184, LPI, Houston, TX.

Warner, N. H., Grant, J. A., Wilson, S. A., Golombek, M. P., DeMott, A., Hauber, E., Ansan, V., Weitz, C., et al. (2020a), An impact crater origin for *Homestead Hollow*, the *InSight* landing site on Mars, *LPSC LI*, 1536, LPI, Houston, TX.

Warner, N. H., Grant, J. A., Wilson, S. A., Golombek, M. P., DeMott, A., Charalambous, C., Hauber, E., Ansan, V., et al. (2020b), An impact crater origin for the *InSight* landing site at *Homestead Hollow*, Mars: Implications for near surface stratigraphy, surface processes and erosion rates, *Journal of Geophysical Research* (this issue).

Weitz, C. M., Grant, J. A., Warner, N. H., Golombek, M. P., Hauber, E., Ansan, V., Wilson, S. A., Charlambous, C., et al. (2019a), Comparison of *InSight Homestead hollow* to *Spirit Laguna hollow*, Eos Transactions, *American Geophysical Union Joint Assembly*, Fall Meeting, Abstract 538848.

Weitz, C. M., Grant, J. A., Warner, N. H., Golombek, M. P., Wilson, S. A., Hauber, E., Ansan, V., Charalambous, C., et al. (2019b), Clast sizes and shapes at the *InSight* landing site, *LPSC L*, 1392, LPI, Houston, TX.

Williams, N., Golombek, M. P., Warner, N. H., Daubar, I. J., Hausmann, R. B, Hauber, E., Ansan, V., Grant, J. A., et al. (2019), Surface alteration from landing *InSight* on Mars and its implications for shallow regolith structure, *LPSC L*, 2781, LPI, Houston, TX.

Wilson, S. A., Warner, N. H., Grant, J. A., Golombek, M. P., DeMott, A., Kopp, M., Berger, L., Weitz, C. M., et al. (2019), Crater retention ages at the *InSight* landing site: Implications for the degradation history of *Homestead hollow*, *LPSC L*, 2161, LPI, Houston, TX.

688 **Table 1. Candidate Impact Craters Considered as the Source of *Rocky Field***

Crater Diameter (m)	Distance from Homestead (m)	Quadrant Around Homestead	Crater Class	Age Relative to Homestead	Approximate Extent Continuous Ejecta (m)[1]	Approximate Ray Orinetation	Approximate Ray Extent (m)[2]	Candidate Source for Rocky Field (as Ejecta or Ray)?
130	700	ENE	5	Younger	130	ENE-WSW	340	No
100	400	ESE	3	Younger	100	ESE-WNW	250	No
80	250	SSE	6	Younger	80	SSE-NNW	190	No
120	200	SSE	7	Older	120	SSE-NNW	300	No
15	15-30	W	8	Younger	15	W-E	20	Yes - E
100	100	NW	6	Younger	100	NW-SE	250	Yes - E
110	280	NW	5	Younger	110	NW-SE	280	Yes - R
125	440	N	7	Younger	125	N-S	330	No
125	510	N	7	Older	125	N-S	330	No

[1] Assuming Continuous Ejecta extends ~1D from the rim (Melosh, 1989)

689 [2] Based on calculation of ray extent (R_t) = $10.5R^{1.25}$ (Baldwin, 1963; Melosh, 1989)

690 Figure 1

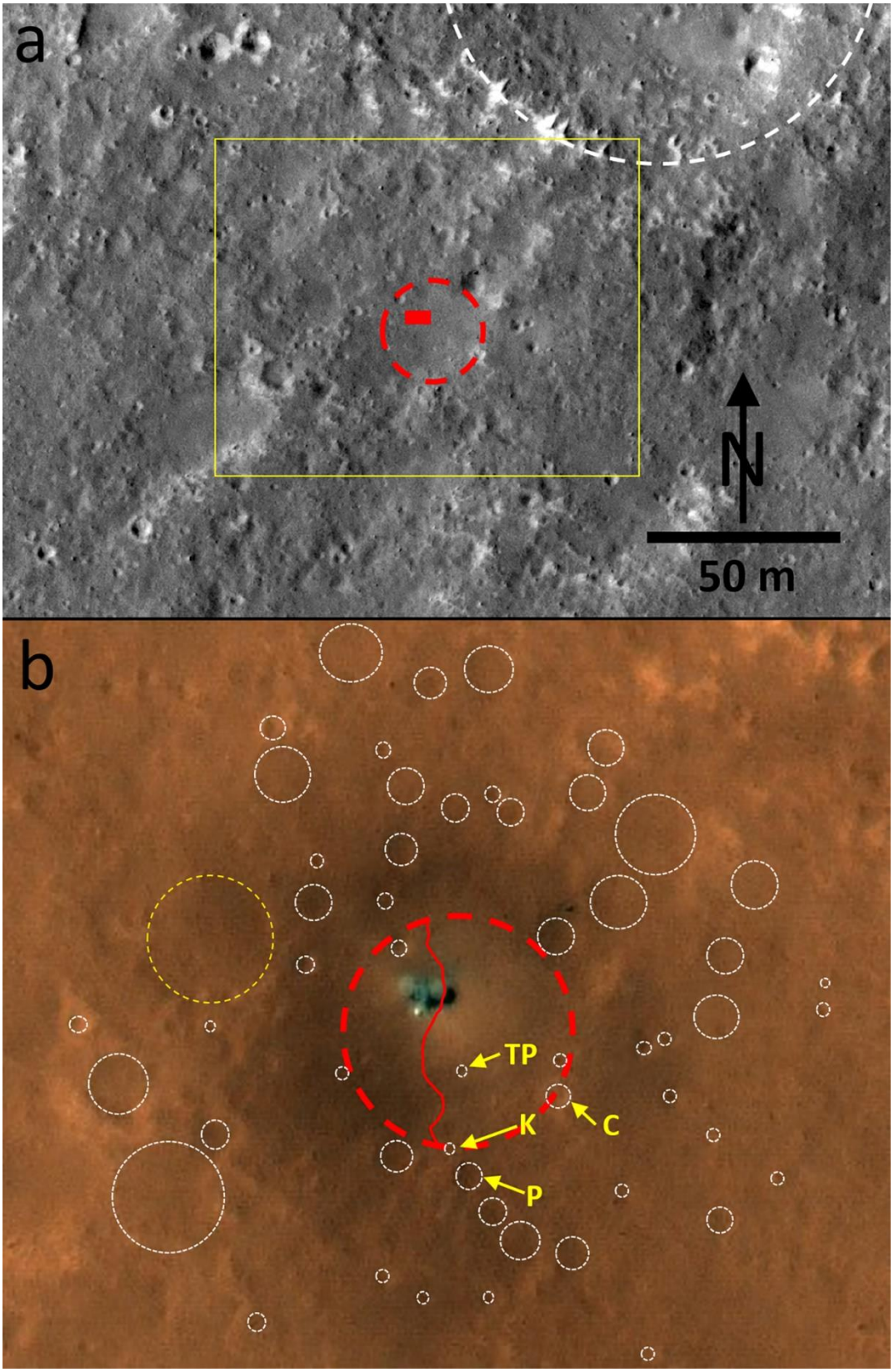

691

Figure 1. (a) The *InSight* lander (red rectangle) is in the northwest corner of the ~27 m-diameter *Homestead hollow* (outlined by red dashed line), one of numerous small craters in varying stages of degradation in Elysium Planitia (4.502°N, 135.623°E; planetocentric coordinates based on HiRISE location georeferenced to the Mars Orbiter Laser Altimeter, Golombek et al., 2019a; 2019b; Parker et al., 2019). The hollow formed ~50 m to the south-southwest of an older, very degraded ~100 m-diameter crater (outlined by white dashed line). Subframe of HiRISE image ESP_036761_1845 (0.25 m/pixel) that is approximately 232 m across and 158 m top to bottom. **(b)** Inset (yellow box in (a)) color view of *InSight* lander in *Homestead hollow* and immediate vicinity. The deployed Seismic Experiment for Internal Structure (SEIS, Lognonné et al., 2019) instrument can be seen as a bright white spot to the south of the lander. For scale, the lander solar panels in (b) span 6 m. Numerous other small craters/quasi-circular depressions or hollows are visible within ~1D of the lander and are indicated by white dashed outlines. These include *Corintito* (C), *The Puddle* (TP), *Kettle* (K), and *Peekaboo* (P) (see Fig. 2) and a ~15 m-diameter degraded hollow to the west (outlined by yellow dashed line, also shown by red line immediately west of the lander in Fig. 6). These frequently correlate with the occurrence smooth, bright deposits (see Fig. 2) similar to those in Homestead hollow. The red line cutting across the hollow is the boundary between occurrence of relatively few rocks to the east versus ~2X-3X more rocks larger than a few cm in the region to the west dubbed "*Rocky Field*." Subframe of HiRISE color image ESP_061684_1845 (0.25 m/pixel).

Figure 2

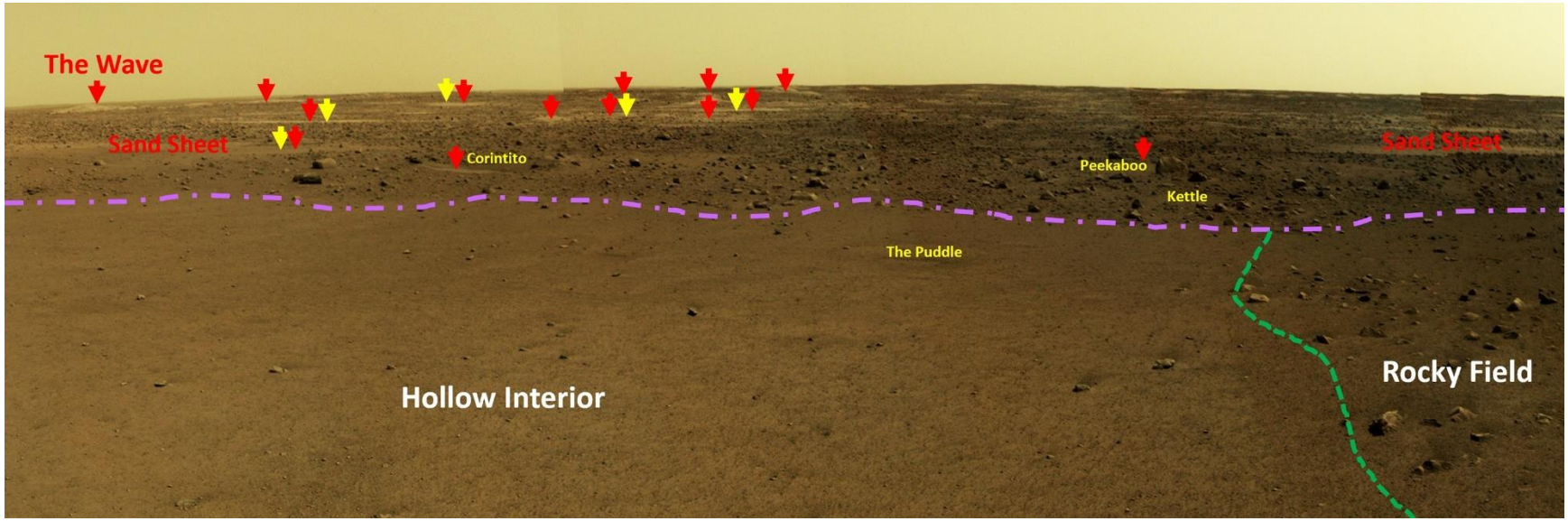

Figure 2. The relatively rock free interior of *Homestead hollow* contrasts with the rockier appearance of the rim, separated by the purple dashed line. The green line inside the hollow marks the boundary between the rock-free interior and portions with ~2X-3X higher rock abundance on the western part of the hollow in *Rocky Field* (see Fig. 1). Evidence of ongoing eolian and impact degradation in and around *Homestead hollow* includes nearby sand sheets within small craters and craterforms/hollows as well as bedforms (red labels and arrows). Yellow arrows and labels indicate smooth bright deposits frequently within nearby impact craters or hollows and associated with probable eolian deposits (by analogy with the sediments in the interior of *Homestead hollow*, see also Fig. 1). View is from approximately 90° to 190° (where 0° is due north) and the *Corintito*, *Peekaboo*, *Kettle*, and *The Puddle* craters are 19 m, 21 m, 16 m, and 8 m from the lander, respectively. At a minimum, *Kettle* and *Corintito* likely ejected small fragments that landed within the hollow. Portion of IDC Mosaic D_LRGB_0014_RAS030100CYL_R__SCIPANQM1.

Figure 3.

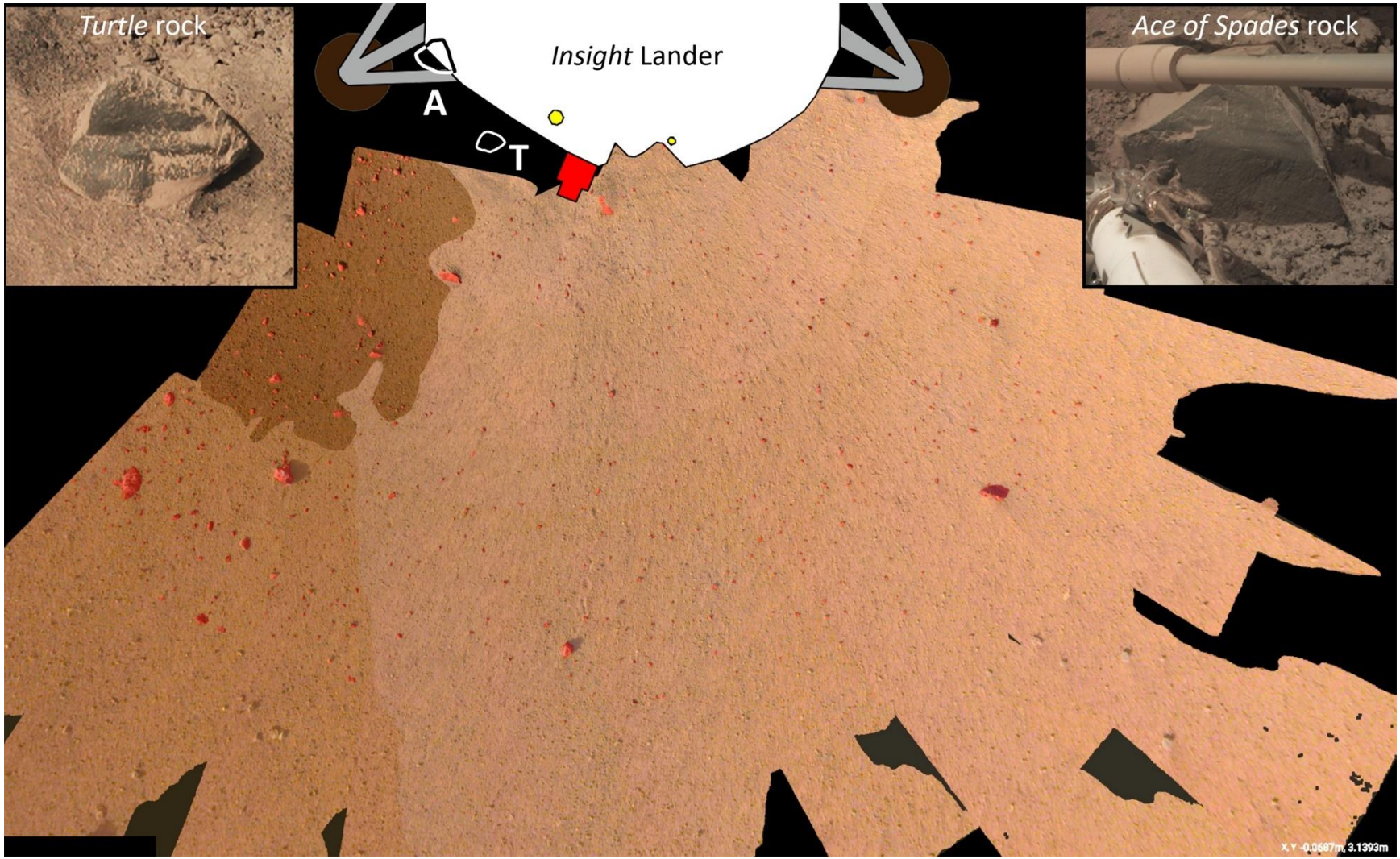

Figure 3. *InSight* WebGIS composite (Calef et al., 2019) of lander workspace and vicinity highlighting the generally fine-grained nature of the surface of *Homestead hollow*. IDC mosaic F2MMWKSSM1 (2 mm pixel-scale) overlain by *InSight* Geology Group map of soils and rocks (red). Medium and dark brown (left side of figure) indicate a medium coarse sand to cobble unit and a coarser sand to pebble

unit, respectively. Rock density is higher in darker brown units, likely due to accumulation of clods excavated by lander rockets during landing (Grant et al., 2019a). The light brown unit is a finer sand to cobble unit. (T) *Turtle* rock (upper left inset, IDC image D001L0014_597774194EDR_F0909_0010M1) and (A) *Ace of Spades* rock (upper right inset, IDC image D000M0014_597773743EDR_F0000_0127M1) are likely ventifacts and are located inboard of the mosaic edge where their approximate outlines are indicated. Radial pattern away from the lander is due to minimal sculpting of the surface by the blast from the lander descent engines during landing. Lander footpad centers ~1.4 m apart. North is towards the top.

Figure 4

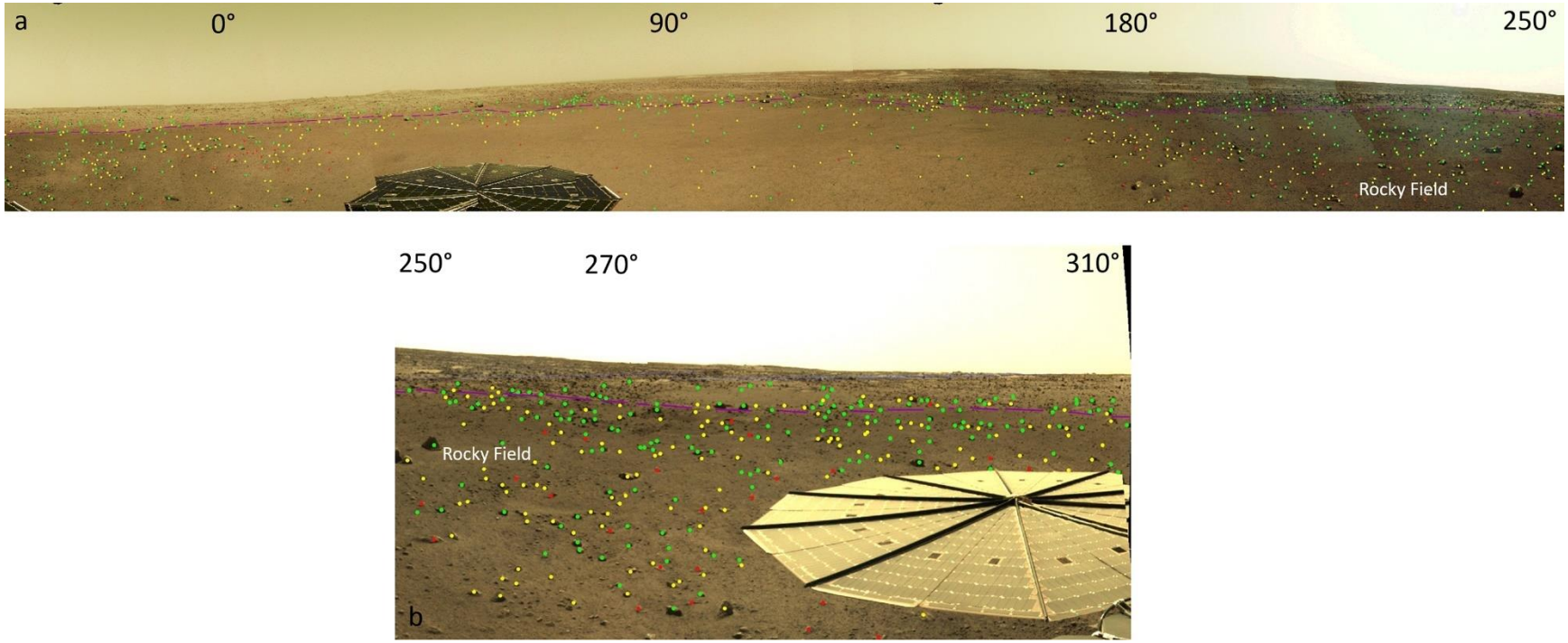

Figure 4. (a) Mosaic covering approximately 290 degrees around the north, east and south side of lander in *Homestead hollow* and **(b)** mosaic covering approximately 70 degrees around the west side of the lander. A total of 1,180 rocks were evaluated over both mosaics based on whether they were mostly exposed and display fairly broad cross-sections and/or some portion of the base was visible (green dots), whether they expose lesser cross-sections and were partially exposed/embedded and embayed by fill with no portion of the base visible (yellow dots), or whether they were mostly buried and so embayed by fill that only a limited cross-section and just the top was visible (red dots). For scale, the lander solar panels in both mosaics are 2.15 m in diameter. The purple dashed line denotes the approximate edge of the hollow. *Rocky Field* denotes the ~2X-3X higher density of rocks on the west-northwest part of the hollow interior. Numbers refer to azimuth where 0° is true north. Mosaic D_LRGB_0014_RAS030100CYL_R__SCIPANQM1 (a) and IDC Mosaic D_LRGB_0119_RAD030100CYL_R__AUTOGENM3 (b). Small black areas around mosaic margins are gores in the image data.

Figure 5

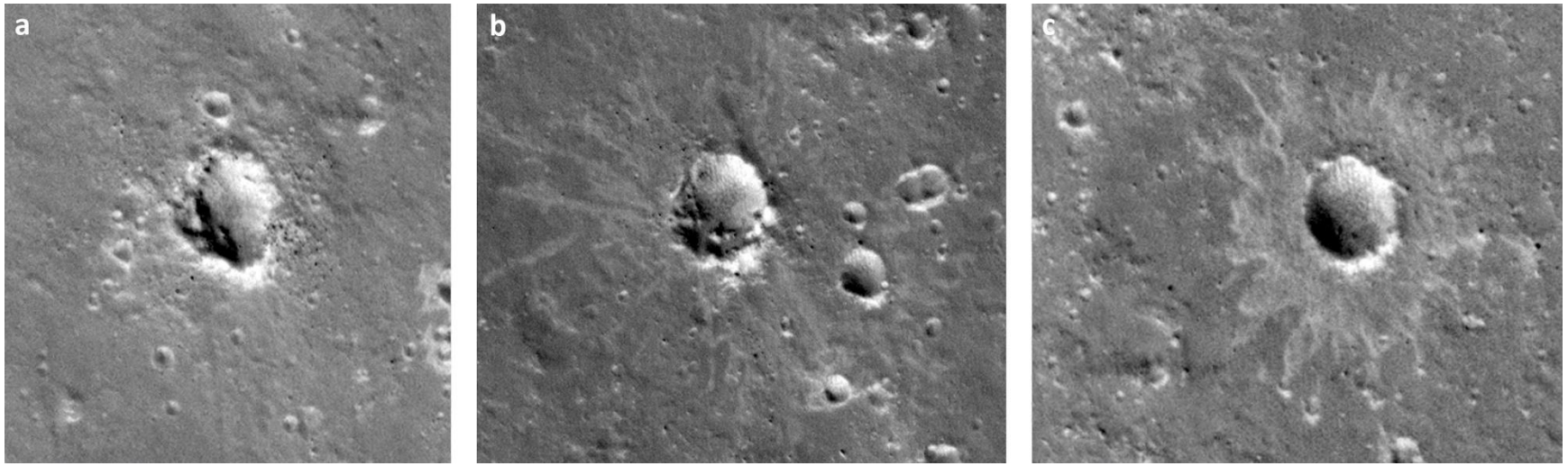

Figure 5. Relatively pristine (Class 2) small craters within 5-6 km of *Homestead hollow*, and of similar size, showing the effects of substrate properties, such as locally variable regolith thickness/properties, on crater form. The absence of pristine (Class 1) craters within 5-6 km of *InSight* highlights the initially high rates of eolian degradation and initial infilling, as evidenced by relatively rock-free, smooth floors sometimes partially capped by ripples (mostly northern third of floor). **(a)** 25 m-diameter crater 4.9 km north-northeast of *InSight* (4.58°N, 135.63°E) with a fairly smooth floor, irregular shape, terraces along a portion of the southwest wall, and surrounded by ejecta with numerous rocks that likely impacted where regolith was relatively thin. **(b)** 28 m-diameter crater 6.7 km northwest of *InSight* (4.60°N, 135.56°E) that is rockier, terraced, and surrounded by rocky ejecta to the south and less rocky ejecta to the north. The northern interior is smoother and expresses ripples. The crater may have impacted into relatively thin regolith to the south and thicker, less rocky (likely sandy based on the absence of detectable rocks, smooth texture, occurrence of eolian ripples, and analogy with the fill within *Homestead hollow*), pre-existing crater-fill to the north. **(c)** 22 m-diameter crater 6.2 southeast of *InSight* (4.41°N, 135.67°E) that is mostly smooth-floored with superposing ripples to the north, symmetrical, and is surrounded by bright, likely sandy ejecta (based on the absence of detectable rocks and smooth texture) largely devoid of large rocks. The crater may have impacted almost entirely into thicker regolith associated with pre-existing, mostly fine-grained, crater-fill. Craters dominated by rocky ejecta likely degrade slower than those dominated by sandy ejecta because deflation leads to faster establishment of surface lags and/or boundary layers that slow further stripping. All craters are in HiRISE image ESP_057939_1845 (0.25 m/pixel) with north towards the top.

Figure 6

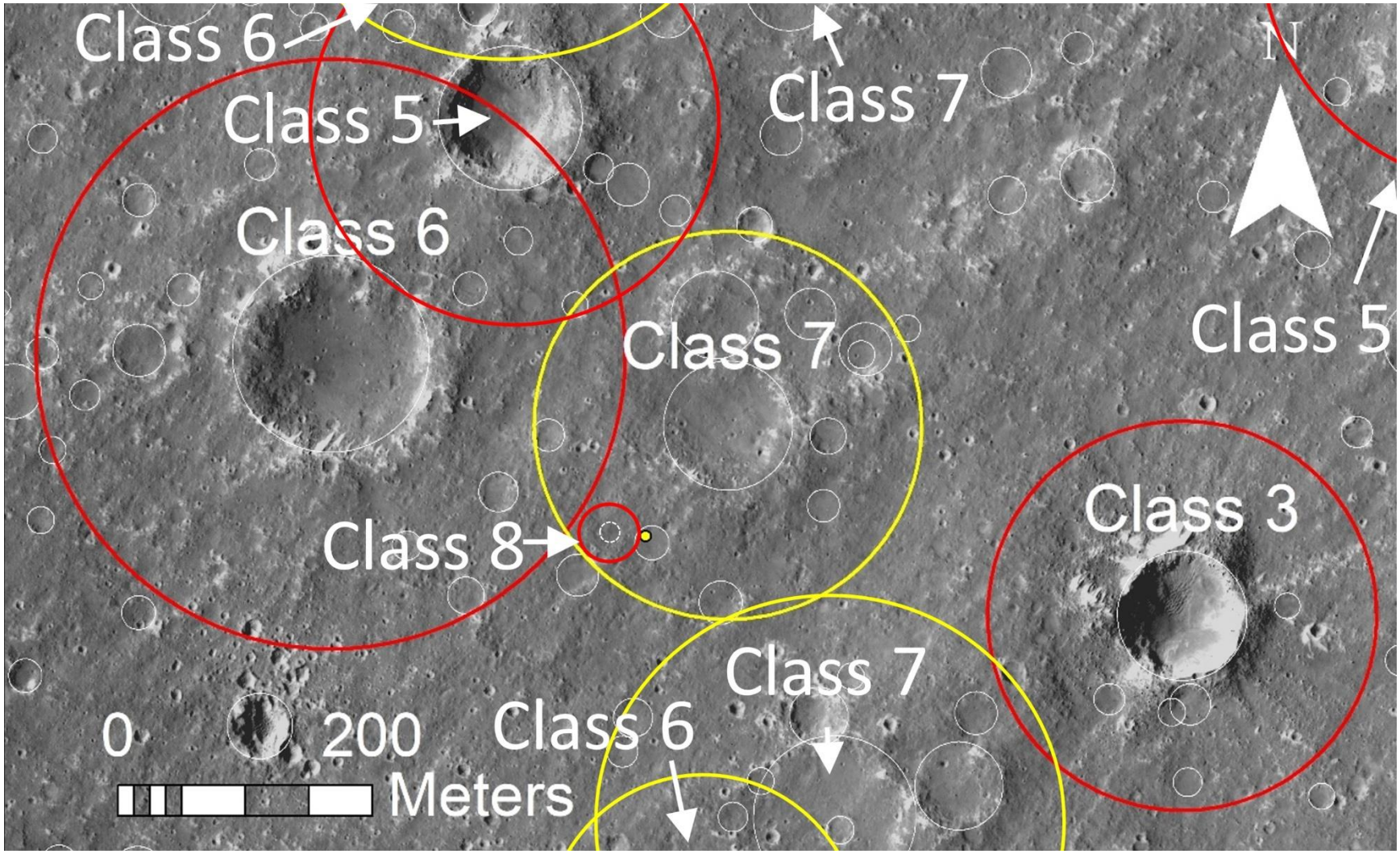

Figure 6. Possible source craters for the rocks forming *Rocky Field* in *Homestead hollow* (the yellow dot is the location of the *InSight* lander in *Homestead* hollow at 4.502°N, 135.623°E). The approximate limit of continuous ejecta associated with craters older than *Homestead hollow* (yellow) and younger (red) than *Homestead hollow* are indicated. White circles denote the rims of all other craters

larger than 20 m in diameter in the vicinity of *Homestead hollow*. Occurrence of *Rocky Field* on the western floor of *Homestead hollow* is consistent with ejecta arriving from either of three source craters (crater class assigned using criteria in Warner et al., 2020a; 2020b) located in quadrant west to northwest of the hollow (Table 1). The ~150 m-diameter Class 6 crater and the 110 m-diameter Class 5 craters to the northwest of *Homestead hollow* are both younger than the hollow. The hollow is close to the expected limit of the continuous ejecta associated with the ~150 m-diameter Class 6 crater, but its discontinuous ejecta may reach the hollow and is the best candidate for *Rocky Field*. The 110 m-diameter Class 5 crater could have produced a ray reaching the hollow with an orientation broadly consistent with the boundary of *Rocky Field*. The ~15 m-diameter crater immediately west of the hollow is also a possible source crater but may be too far away to account for the entire extent of *Rocky Field*. The 100 m-diameter Class 3 crater and the 130 m-diameter Class 5 crater to the east-southeast and east northeast, respectively, are younger but too far away to have sourced *Rocky Field* (Table 1). The Class 6 craters to the north and south of the hollow are likely younger than the hollow, but both are too far away to have provided rocks as either ejecta or rays. The Class 7 craters to the north and south of the hollow (most of crater and likely extent of continuous ejecta partially shown for the crater to the south) both predate the hollow and could not have sourced *Rocky Field*. The ~100 m-diameter Class 7 crater (Warner et al., 2020a; 2020b) immediately to the northeast of *Homestead hollow* predates the hollow and the remains of its distal continuous ejecta (~10's of cm) was likely excavated during hollow formation. Subframe of HiRISE image ESP_036761_1845 (0.25 m/pixel) that is approximately 1100 m across and 667 m from top to bottom, with north towards the top.

Figure 7

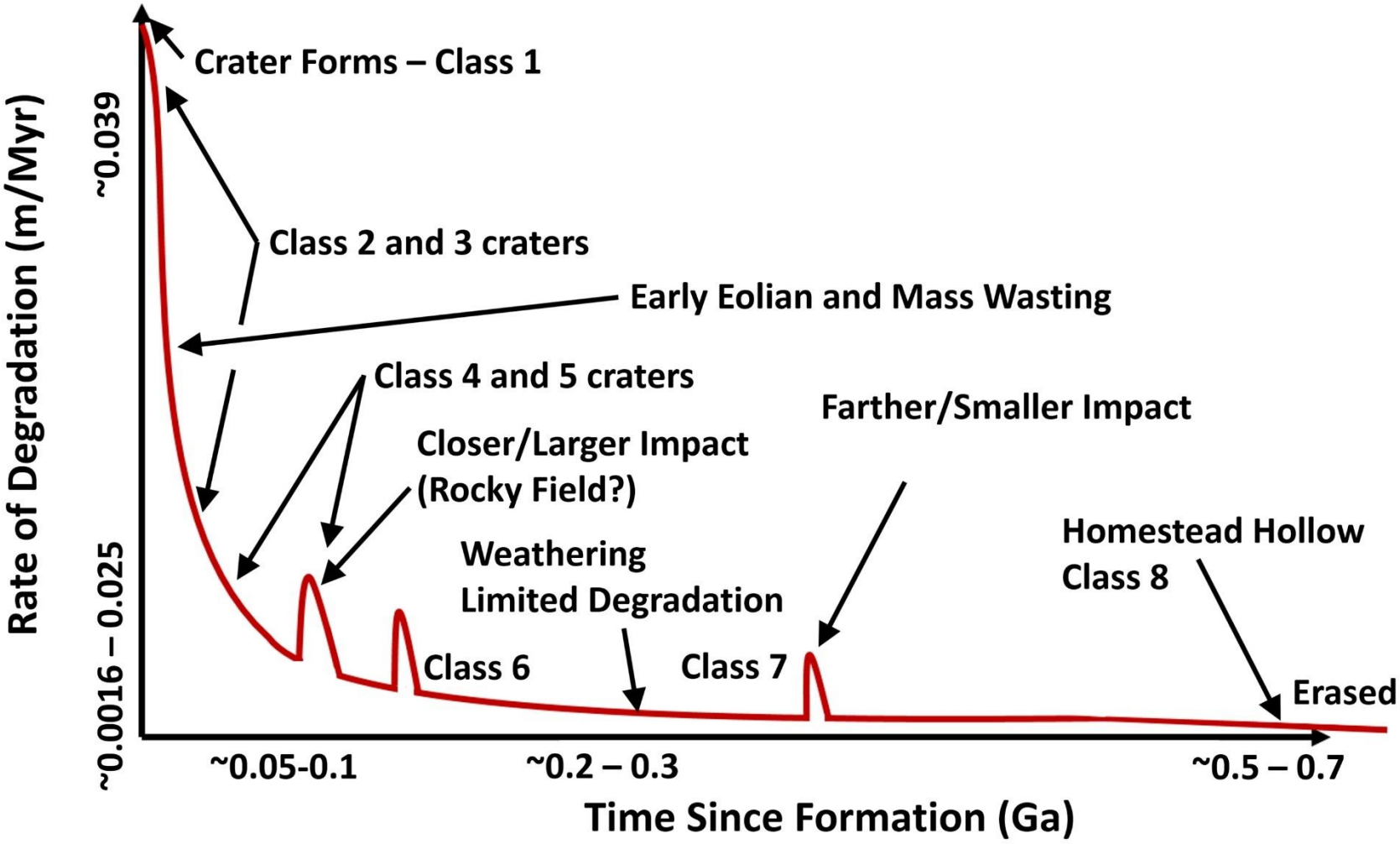
Crater Forms – Class 1
Class 2 and 3 craters
Early Eolian and Mass Wasting
Class 4 and 5 craters
Farther/Smaller Impact
Closer/Larger Impact
(Rocky Field?)
Homestead Hollow
Class 8
Weathering
Limited Degradation
Class 6
Class 7
Erased
Rate of Degradation (m/Myr)
~0.039
~0.0016 – 0.025
~0.05-0.1
~0.2 – 0.3
~0.5 – 0.7
Time Since Formation (Ga)

Figure 7. Idealized degradation timeline for *Homestead hollow* and similar-sized craters in the vicinity of the *InSight* lander. Pristine craters expose deposits of mixed coarse and mostly fine ejecta that are in disequilibrium with local geomorphic thresholds and undergo relatively rapid degradation by eolian and lesser mass-wasting processes. The early degradation results in Class 5 morphologies appearing within ~0.1 Ga of formation. Subsequent degradation leading to more degraded Class 6 to Class 8 morphologies (on order of 0.3-0.6 Ga) is much slower and mostly limited by introduction of small inventories of fines following nearby impact events and the very slow weathering of resistant basaltic rocks in and around the hollow. Random impacts in or nearby the hollow can also emplace ejecta within the hollow (e.g., *Rocky Field*). Nevertheless, most of these small craters only contribute to further gardening of the uppermost meter or so of the near-surface and don't excavate new rocks from greater depths in the regolith. Occurrence of likely duricrust within the uppermost fill of *Homestead hollow* (Golombek et al., 2019b; 2020) highlights the relative stability of the interior surface at advanced stages of degradation and when the surface properties and profile are near or in equilibrium with respect to local geomorphic thresholds. Degradation rates and retention times are adopted from Warner et al. (2020a; 2020b).